In Vivo Quantification of Brain Serotonin Transporters in Humans Using [^{11}C]McN 5652

Ramin V. Parsey, Lawrence S. Kegeles, Dah-Ren Hwang, Norman Simpson, Anissa Abi-Dargham, Osama Mawlawi, Mark Slifstein, Ronald L. Van Heertum, J. John Mann, and Marc Laruelle

Departments of Psychiatry and Radiology, Columbia University College of Physicians and Surgeons, New York; and Division of Brain Imaging, Department of Neuroscience, New York State Psychiatric Institute, New York, New York

Abnormal brain regional densities of serotonin (5-hydroxytryptamine [5-HT]) transporters have been reported in postmortem studies in several neuropsychiatric conditions, such as major depression and schizophrenia. *trans*-1,2,3,5,6,10-β-Hexahydro-6-[4-(methylthio)phenyl]pyrrolo-[2,1-a]-isoquinoline ([^{11}C]McN 5652) is the first PET radioligand successfully developed to label 5-HT transporters in the living human brain. The purpose of this study was to develop an imaging protocol and analytic method to measure regional 5-HT transporter binding potential (BP) with [^{11}C]McN 5652 in humans. **Methods:** The arterial input function and brain uptake of (+)-[^{11}C]McN 5652 and (−)-[^{11}C]McN 5652, the active and inactive enantiomers, respectively, were measured in 6 healthy volunteers. **Results:** (+)-[^{11}C]McN 5652 concentrated in brain regions rich in 5-HT transporters (midbrain, thalamus, basal ganglia, and medial temporal lobe structures), whereas the uptake of (−)-[^{11}C]McN 5652 was more uniformly distributed. Total distribution volumes (V_T) were derived using kinetic 2-compartment analysis and graphic analysis. V_T derived by both methods were highly correlated. (+)-[^{11}C]McN 5652 regional V_T ranged from 18 ± 2 mL/g in the cerebellum to 46 ± 13 mL/g in the midbrain. (−)-[^{11}C]McN 5652 regional V_T ranged from 10 ± 2 mL/g in the cerebellum to 14 ± 3 mL/g in the thalamus. (+)-[^{11}C]McN 5652 V_T were higher than (−)-[^{11}C]McN 5652 V_T in all regions, including the cerebellum, a region devoid of 5-HT transporters. Blocking experiments were also performed in baboons with saturating doses of citalopram and in humans with nonsaturating doses of paroxetine. Cerebellar and neocortical (+)-[^{11}C]McN 5652 V_T were unaffected by pretreatment with 5-HT transporter blockers. In areas of high receptor concentration (midbrain, caudate, and thalamus) 5-HT transporter blockers decreased (+)-[^{11}C]McN 5652 V_T to the level of cerebellum (+)-[^{11}C]McN 5652 V_T. **Conclusion:** These experiments indicate that the use of the difference between (+)- and (−)-[^{11}C]McN 5652 V_T to define specific binding to 5-HT transporters leads to an overestimation of specific binding. 5-HT transporter BP was derived as the difference between the regional and cerebellar (+)-[^{11}C]McN 5652 V_T. BP values were in good agreement with the distribution of 5-HT transporters in the human brain, except for regions of relatively low 5-HT transporter concentration, such as the prefrontal cortex, where no specific binding was detected using (+)-[^{11}C]McN 5652. (+)-[^{11}C]McN 5652 is an appropriate radiotracer to quantify 5-HT transporters in regions with relatively high concentration of 5-HT transporters, such as the midbrain, thalamus, and basal ganglia, and should prove useful in elucidating abnormalities of 5-HT transmission in neuropsychiatric conditions.

Key Words: serotonin transporter; PET; [^{11}C]McN 5652; human brain; selective serotonin reuptake inhibitors

J Nucl Med 2000; 41:1465–1477

Alterations of serotonin (5-hydroxytryptamine [5-HT]) transmission have been implicated in numerous psychiatric disorders (*1,2*). 5-HT transporters, located on presynaptic terminals, terminate the action of 5-HT by reuptake into the presynaptic neuron (*3*). Because of their localization on the 5-HT nerve terminals, the density of these sites is a marker of the number or integrity of 5-HT terminals. Thus, the ability to measure 5-HT transporters in vivo with PET is critical in characterizing putative abnormalities of 5-HT transmission in psychiatric disorders.

trans-1,2,3,5,6,10-β-Hexahydro-6-[4-(methylthio)phenyl]-pyrrolo-[2,1-a]-isoquinoline (McN 5652) is a promising PET radiotracer for labeling 5-HT transporters (*4,5*). In vitro, the active enantiomer (+)-McN 5652 is a selective and potent (dissociation constant [K_d] = 0.4 nmol/L) inhibitor of 5-HT uptake (*6*). The in vivo brain regional distribution of (+)-[^{11}C]McN 5652 in rats (*4*), baboons (*7*), and humans (*8*) correlates with known regional concentrations of 5-HT transporters, and the specific uptake of (+)-[^{11}C]McN 5652 is blocked after pretreatment with the 5-HT reuptake blocker fluoxetine. In contrast, the brain uptake of the inactive enantiomer (−)-[^{11}C]McN 5652 is relatively uniform across brain regions (*4,7,8*).

Although considerable evidence supports the potential of (+)-[^{11}C]McN 5652 as a PET 5-HT transporter radiotracer, important methodologic questions remain to be addressed. The goal of this study was to evaluate the potential of (+)-[^{11}C]McN 5652 to provide quantitative information about 5-HT transporter density in various regions of the human brain and to derive appropriate scanning and analytic protocols. Several model-based methods were compared for derivation of the binding potential (BP; number of available binding sites [B_{max}]/K_d) of 5-HT transporters in humans using the active (+) and inactive (−) enantiomers of

Received Jul. 2, 1999; revision accepted Jan. 19, 2000.

For correspondence or reprints contact: Ramin V. Parsey, MD, PhD, New York State Psychiatric Institute, 1051 Riverside Dr., Box 42, New York, NY 10032.

[^{11}C]McN 5652. Specifically, we attempted to determine the minimal scanning time, the optimal method of analysis, the value of using the inactive enantiomer (−)-[^{11}C]McN 5652 for determination of regional nonspecific binding, and the detectability of specific binding to 5-HT transporters in regions with relatively low densities, such as neocortical regions.

The brain uptake of active and inactive McN 5652 was studied on the same day in 6 healthy volunteers (control experiments). On completion of these studies, additional information on the proper definition of nonspecific binding was obtained from experiments in baboons after citalopram pretreatment and in humans after paroxetine pretreatment (blocking experiments).

MATERIALS AND METHODS

Subjects

Six healthy male volunteers participated in this study (mean age ± SD, 38 ± 12 y). The absence of present or past psychiatric, neurological, and significant medical disorders was assessed by history, review of systems, physical examination, routine blood tests, urine toxicology, and electrocardiogram. All subjects were free of medication for at least 2 wk before the study. The study was approved by Columbia Presbyterian Medical Center institutional review board, and subjects provided written informed consent after receiving an explanation of the study. Six studies were also performed in 1 baboon under isoflurane anesthesia. Anesthesia induction, maintenance, and monitoring were performed as described (*9*).

Radiochemistry

The butyryl thioester precursor for the synthesis of [^{11}C]McN 5652 was prepared by demethylating the (+)- or (−)-McN 5652 with sodium thiomethoxide in anhydrous dimethylformamide (DMF) at 165°C for 1.5 h followed by adding butyryl chloride to give the butyryl thioester (*10*). The crude butyl thioester was purified by semipreparative high-performance liquid chromatography (HPLC) according to Suehiro et al. (*10*). The purified butyryl thioester (1 mg) was transferred as a solution in methylene chloride into a 1-mL vial, and 0.5 mg tartaric acid was added to stabilize the butyryl thioester. The solution was concentrated under a stream of nitrogen to dryness, and the vial was capped and stored in a −20°C freezer.

For radiolabeling, 1 vial of the butyryl thioester tartrate precursor was treated with tetrabutyl ammonium hydroxide (10 μL, 1 mol/L in methanol) at room temperature for 10 min and then diluted with 0.3 mL anhydrous DMF. The reaction solution was cooled in an ice bath. [^{11}C]Methyl iodide (prepared using a 1-pot procedure: trapping [^{11}C]CO_2 in a tetrahydrofuran solution of lithium aluminum hydride followed by reacting with concentrated HI) was distilled by a stream of argon into the DMF solution. The mixture was heated for 2 min at 40°C, mixed with 0.5 mL HPLC solvent, and purified by HPLC (Prodigy ODS column, 10 μm; Phenomenex, Torrance, CA; 10 × 250 mm; 40:60 acetonitrile (ACN)/0.1 mol/L ammonium formate, 10 mL/min). The product had a retention time of 12 min.

The HPLC product fraction was diluted with deionized water to a volume of 50 mL and passed through a C8 SepPak column (Waters, Milford, MA) (preconditioned with 5 mL ethanol and 5 mL water). The SepPak was washed with water, and the product was recovered by elution of the SepPak with 1 mL ethanol. A small amount of the ethanol product solution was injected onto an analytic column (Prodigy ODS(3) column, 5 μm; Phenomenex; 4.6 × 250 mm; 70:30 ACN/aqueous triethylamine, pH 7.4, 2 mL/min) to determine the radiochemical purity (>99%), chemical purity (>95%), and specific activity (SA). The ethanol solution was then diluted with saline (9 mL), filtered through a 0.22-μm membrane filter (GV membrane filter, 25 mm; Millipore, Bedford, MA), and collected in a sterile vial.

For (+)-[^{11}C]McN 5652 (n = 8), the SA at the time of injection was 51 ± 27 Bq/mol (range, 14–124 Bq/mol), the injected dose (ID) was 580 ± 128 MBq (range, 266–706 MBq), and the injected mass was 13.3 ± 4.4 nmol (range, 5.5–20.8 nmol). For (−)-[^{11}C]McN 5652 (n = 8), the SA was 44 ± 19 Bq/mol (range, 7–84 Bq/mol), the ID was 625 ± 88 MBq (range, 496–736 MBq), and the injected mass was 18.6 ± 16.1 nmol (range, 7.5–72.3 nmol). In baboon studies (n = 6), for (+)-[^{11}C]McN 5652, the SA was 125 ± 136 Bq/mol (range, 45–282 Bq/mol), the ID was 559 ± 81 MBq (range, 466–603 MBq), and the mass was 8.32 ± 5.51 nmol (range, 2.20–12.9 nmol). For (−)-[^{11}C]McN 5652, the SA was 138 ± 116 Bq/mol (range, 62–272 Bq/mol), the ID was 581 ± 63 MBq (range, 522–651 MBq), and the mass was 6.38 ± 4.25 nmol (range, 2.08–10.6 nmol).

PET Protocol

After completion of the Allen test and subcutaneous administration of 1% lidocaine, a catheter was inserted in the radial artery. A venous catheter was inserted in a forearm vein on the opposite side. Four fiducial markers filled with ^{11}C (about 74 kBq/per marker at the time of injection) were glued on the subject's head. Head movement minimization was achieved with a polyurethane head immobilizer system (Soule Medical, Tampa, FL), molded around the head of the subject. This system provides better restraint than a thermoplastic mask (O. Mawlawi, unpublished data, January 1999).

PET imaging was performed with the ECAT EXACT 47 scanner (Siemens/CTI, Knoxville, TN) (*11*) (47 slices covering an axial field of view of 16.2 cm, axial sampling of 3.375 mm, 3-dimensional mode in plane and axial resolution of 6.0- and 4.6-mm full width half maximum at the center of the field of view (FOV), respectively). A 15-min transmission scan was obtained before radiotracer injection.

[^{11}C]McN 5652 was injected intravenously as a bolus over a 45-s period of time. After injection of (+)-[^{11}C]McN 5652, emission data were collected in 3-dimensional mode for 150 min as 24 successive frames of increasing duration (3 × 20 s, 3 × 1 min, 3 × 2 min, 2 × 5 min, and 13 × 10 min). After injection of (−)-[^{11}C]McN 5652, emission data were collected in the 3-dimensional mode for 90 min as 18 successive frames of increasing duration (3 × 20 s, 3 × 1 min, 3 × 2 min, 2 × 5 min, and 7 × 10 min). Images were reconstructed to a 128 × 128 matrix (pixel size of 2.5 × 2.5 mm^2). Reconstruction was performed with attenuation correction using the transmission data and a Sheppe 0.5 filter (cutoff, 0.5 cycle per projection ray). Subjects rested outside of the camera for 15–30 min between injections.

Input Function Measurement

After radiotracer injection, arterial samples were collected every 5 s with an automated sampling system for the first 2 min and manually thereafter at longer intervals. Totals of 32 and 29 samples were obtained per experiment for (+)-[^{11}C]McN 5652 and (−)-

[^{11}C]McN 5652, respectively. After centrifugation (10 min at 1800*g*), plasma was collected in 200-μL aliquots, and radioactivity was measured in a 1480 Wizard 3M automatic γ counter (Wallac, Turku, Finland). γ counter efficiency was calibrated at regular intervals with the PET camera using an ^{18}F solution. In addition, a long-lived source (^{22}Na) was counted with each set of samples to control for between-run variance in counting efficiency.

Six samples (collected at 2, 8, 16, 30, 50, and 70 min) were further processed by HPLC to measure the fraction of plasma activity representing unmetabolized parent compound. C_{18} SepPak (Waters classic; Waters) was preconditioned with 5 mL methanol and 10 mL water. One-milliliter aliquots of plasma were loaded onto SepPak cartridges. SepPak were flushed with 1 mL air, washed with 5 mL water, and eluted with 1 mL methanol. A Prodigy ODS(3) column (4.6 × 250 mm, 10 μm) was used and the column was eluted with a 70:30 mixture of ACN/aqueous triethylamine (phosphoric acid, pH 7.4) at a flow rate of 2 mL/min. An in-line Bioscan flow cell γ detector (Bioscan, Washington, DC) was used to monitor the radioactivity. The eluant was collected as 6 4-mL fractions over 12 min, and radioactivity in all collections was measured.

No overlap was observed between metabolite (first 4 min) and parent (7.8 min) peaks. Two fractions (fractions 4 and 5) were needed to ensure collection of the entire parent peak (this was true for both standards and samples). No radioactive peaks were detected after the parent peak. For each sample, the parent fraction was estimated by the ratio of decay-corrected activity in fractions 4 and 5 to the activity of the total collection. The percentage parent peaks calculated using the counts from the well counter were in agreement with the numbers obtained from the HPLC integration. However, at late time points, because of the low signal-to-noise ratio obtained from the flow cell detector, the well counter method was more reliable. A control blood sample with standard [^{11}C]McN 5652 solution was processed with each experiment.

A biexponential function was fitted to the 6 measured parent fractions and used to interpolate values between and extrapolate values after the measurements. The smallest exponential of the parent fractions curve, λ_{par}, was constrained to the difference between λ_{cer}, the terminal rate of washout of cerebellar activity, and λ_{tot}, the smallest elimination rate constant of the total plasma (*9*). The input function was calculated as the product of total plasma counts and interpolated parent fraction at each time. The measured input function values, (C_a(t), kBq/mL), were fitted to a sum of 3 exponentials, and the fitted values were used as input to the kinetic and graphic analyses. The clearance of the parent compound (C_L, L/h) was calculated as the ratio of the injected dose to the area under the curve of the input function (*12*). Determination of the [^{11}C]McN 5652-free fraction in the plasma with an ultracentrifugation technique (*13*) was impaired by the high retention (>90%) of free [^{11}C]McN 5652 on the filter and was not obtained in these studies.

MRI Acquisition and Segmentation Procedures

MRI was performed on a 1.5-T Signa Advantage system (General Electric Medical Systems, Milwaukee, WI). After obtaining a sagittal scout (localizer) film to identify the anterior commissure–posterior commissure (AC–PC) plane (1 min), a transaxial T1-weighted sequence with 1.5-mm slice thickness was acquired in a coronal plane orthogonal to the AC–PC plane over the whole brain with the following parameters: 3-dimensional spoiled gradient-recalled acquisition in the steady state; repetition time, 34 ms; echo time, 5 ms; flip angle, 45°; slice thickness, 1.5 mm and zero gap; 124 slices; FOV, 22 × 16 cm; 256 × 192 matrix, reformatted to 256 × 256, yielding a voxel size of 1.5 × 0.9 × 0.9 mm; and time of acquisition, 11 min. MRI segmentation was performed as described (*14*).

Image analysis was performed with MEDx (Sensor Systems Inc., Sterling, VA) according to the following steps: frame realignment, PET–MRI registration, and time–activity curve measurement. First, to correct for head movement during the acquisition, all frames were coregistered to the first frame of the study using automated image registration (AIR) (*15*). Because of the performance of the head-restraining device, very little movement correction was needed (<1-mm motion in all axes measured between frames). Second, after frame-to-frame registration, the 21 frames were summed, and the summed PET image was coregistered to the MR image and resampled using AIR. The parameters of the spatial transformation matrix of the summed PET dataset were then applied to each individual frame. Third, region-of-interest (ROI) boundaries were drawn on the MR image according to criteria on the basis of brain atlases (*16,17*) and published reports (*18,19*). Neocortical regions included dorsolateral prefrontal cortex (DLPFC), medial prefrontal cortex (MPFC), orbitofrontal cortex (OFC), subgenual prefrontal cortex (SPFC), anterior cingulate cortex (ACC), parietal cortex (PC), temporal cortex (TC), and occipital cortex (OC). Subcortical regions included caudate (CAU), putamen (PUT), thalamus (THA), amygdala (AMY), hippocampus (HIP), midbrain (MID), and cerebellum (CER). The region referred to as the MID includes various structures with dense 5-HT transporter concentration (raphe nuclei, substantia nigra, locus coeruleus, ventral tegumental area, and superior and inferior colliculi). Two methods were used for final ROI definition. A segmentation-based method was used for neocortical regions and the CER, and a direct identification method was used for subcortical regions. For neocortical regions, large regions were first drawn to delineate the boundaries of the ROIs. Within these regions, only gray matter (GM) voxels were used to measure activity distribution. Because of the mixture of GM and white matter in central gray structures, the segmentation-based approach was not used to define subcortical ROIs.

Derivation of Regional Total Distribution Volumes

Derivation of [^{11}C]McN 5652 regional distribution volumes was performed using kinetic and graphic analyses. Kinetic analyses were performed using a 3-compartment model (3-CPT model) or a 2-compartment model (2-CPT model). The 3-CPT configuration included the arterial plasma compartment (C_a), the intracerebral free and nonspecifically bound compartment (nondisplaceable compartment, C_2), and the specifically bound compartment (C_3). The 2-CPT configuration included the arterial plasma compartment (C_a) and 1 tissue compartment (C_T) that included the intracerebral free, nonspecifically bound and specifically bound compartments. Brain activity was corrected for the contribution of plasma activity assuming a 5% blood volume in the ROIs (*20*).

The total regional distribution volume (mL of plasma/g of tissue) was defined as the ratio of the tracer concentration in this region to the metabolite-corrected plasma concentration at equilibrium:

$$V_T = \frac{C_T}{C_a}, \qquad \text{Eq. 1}$$

where V_T is total distribution volume.

Kinetic derivations of the V_T were obtained as:

$$V_T = \frac{K_1}{k_2'} \quad \text{Eq. 2}$$

and

$$V_T = \frac{K_1}{k_2}\left(1 + \frac{k_3}{k_4}\right) \quad \text{Eq. 3}$$

for the 2-CPT and 3-CPT configurations, respectively, where K_1 (mL/g/min) and k_2 (min^{-1}) are the unidirectional fractional rate constants for the transfer between C_a and C_2, k_3 (min^{-1}) and k_4 (min^{-1}) are the unidirectional fractional rate constants for the transfer between C_2 and C_3, and k_2' (min^{-1}) is the fractional rate constant for the transfer from C_T to C_a ($k_2' = k_2/(1 + k_3/k_4)$) (*21,22*).

Kinetic parameters were derived as described (*21*). The goodness of fit of models with different levels of complexity was compared using the Akaike information criterion (AIC) (*23*) and the F test (*24,25*). The identifiability of model parameters was assessed by the SE of the parameters at convergence, given by the diagonal of the covariance matrix (*25*), and expressed as percentage of the parameters (coefficient of variation, %CV). Graphic derivation of the V_T was obtained using the method of Logan et al. (*26*).

The relationship between (+)-[^{11}C]McN 5652 V_T derivation and the duration of the scan was evaluated by analyzing shorter duration datasets (140, 130, 120, 110, 100, 90, 80, 70, and 60 min) and comparing the results with the reference value obtained with the 150-min dataset. For each region and duration, V_T was expressed as percentage of the reference value. Under these conditions, the mean ± SD of the V_T provides an estimate of the bias (mean) and dispersion (SD) induced in the outcome measure by reducing the duration of the scans. The solution was considered stable after time t if all results derived from time t to the end of the experiment had a mean within 10% of the reference value and a SD that did not exceed 10%.

Derivation of Specific Distribution Volume

Kinetic and graphic analyses were used to calculate the V_T, which is the sum of the specific and nondisplaceable (free plus nonspecific binding) distribution volumes. Two methods were available to estimate the nondisplaceable distribution volume, either as the V_T of the inactive enantiomer (enantiomer method) or as the V_T of the active enantiomer in the CER, a region with negligible concentration of 5-HT transporters (region-of-reference method). The enantiomer method has the potential advantage of taking into account region differences in nondisplaceable distribution volumes. However, this method requires demonstration that the nondisplaceable distribution volume of the active enantiomer is equal to the V_T of the inactive enantiomer. Blocking experiments were performed to evaluate this assumption.

Because of the difficulty in achieving complete saturation of 5-HT transporters in humans, blocking studies were initially performed in 1 baboon (male *Papio anubis*, 12 kg) using citalopram. Three experiments were performed on the same animal. The first experiment included sequential injections of (+)- and (−)-[^{11}C]McN 5652 under control conditions. The second experiment included sequential injections of (−)-[^{11}C]McN 5652, citalopram (4 mg/kg intravenously at the end of the (−)-[^{11}C]McN 5652 scan), and (+)-[^{11}C]McN 5652 (20 min after citalopram). The third experiment was similar to the second experiment, except that a higher dose (6 mg/kg) of citalopram was used. The doses of citalopram used in these studies (4–6 mg/kg) have been shown to result in complete displacement of [^{123}I]-2β-carbomethoxy-3β-(4-iodophenyl)-tropane ([^{123}I]β-CIT) from the MID 5-HT transporters in baboons (*27*). Thus, these experiments were optimized to compare the distribution volumes of (−)-[^{11}C]McN 5652 under control conditions with the distribution volumes of (+)-[^{11}C]McN 5652 under complete blockade of 5-HT transporters.

To confirm results obtained in the baboon experiments, blocking studies were also performed in humans under conditions of partial receptor blockade. Two of the 6 volunteers were invited to repeat the scanning procedure (sequential (+)-[^{11}C]McN 5652 and (−)-[^{11}C]McN 5652 scans). Subjects were pretreated with paroxetine. The first subject was given 20 mg paroxetine orally 6 h before and 40 mg 3 h before the radiotracer injection (total dose, 60 mg). The second subject received 40 mg paroxetine orally 6 h before and 3 h before the radiotracer injection (total dose, 80 mg). These doses should correspond to a plasma level of ~25–35 ng/mL at the time of the scan (*28*). No adverse effects were noted or reported by the subjects.

After appropriate definition of the nondisplaceable distribution volume (V_2), 2 measures of specific distribution volumes were derived: BP and the equilibrium specific to nonspecific partition coefficient (V_3'').

BP was derived as the difference between total and nondisplaceable distribution volumes:

$$BP = V_T - V_2. \quad \text{Eq. 4}$$

BP is related to B_{max} and K_d by:

$$BP = \frac{f_1 B_{max}}{K_d}, \quad \text{Eq. 5}$$

where f_1 is the free fraction in the plasma (not measured in this study).

V_3'' was calculated as:

$$V_3'' = \frac{V_T}{V_2} - 1. \quad \text{Eq. 6}$$

V_3'' is related to B_{max} and K_d by:

$$V_3'' = \frac{f_2 B_{max}}{K_d}, \quad \text{Eq. 7}$$

where f_2 is the free fraction in the brain ($f_2 = 1/V_2$). Because f_1 was not measured, f_2 could not be derived.

RESULTS

Control Experiments in Humans

Plasma Analysis. At 30 min, 59% ± 10% of the activity corresponded to the parent active enantiomer and 48% ± 16% corresponded to the inactive enantiomer. No significant differences were observed in the parent fraction between the active and inactive enantiomers (repeated-measures ANOVA: $F_{1,35} = 0.47$, $P = 0.43$). Average plasma clearances of the parent compounds were 162 ± 42 L/h and 148 ± 41 L/h for (+)- and (−)-[^{11}C]McN 5652, respectively, and were not significantly different (repeated-measures ANOVA: $F_{1,5} = 0.20$, $P = 0.66$).

Brain Uptake of (+)-[^{11}C]McN 5652. After injection of (+)-[^{11}C]McN 5652, activity gradually concentrated mostly in the basal ganglia, THA, and MID (Fig. 1). Activities peaked early (around 20 min) in the CER and neocortical regions and later (around 40 min) in the basal ganglia and THA (Fig. 2). MID activity continued to increase until about 60 min and showed a more protracted peak and slower washout rate compared with other regions. During the last 40 min of the scan (110- to 150-min interval), regional-to-cerebellar activity ratios averaged 1.73 ± 0.14, 2.08 ± 0.22, 1.86 ± 0.17, and 2.00 ± 0.22 in the CAU nucleus, PUT, THA, and MID, respectively.

Results of kinetic and graphic analyses are presented in Table 1. Convergence was achieved in all regions (n = 15) and all subjects (n = 6) with the 2-CPT model, but the 3-CPT model failed to converge in 4 of 90 instances. The 3-CPT model provided a slightly but significantly better fit than the 2-CPT model. The AIC were higher for 2-CPT fits (−61 ± 22) than for 3-CPT fits (−78 ± 22; repeated-measures ANOVA: $F_{1,85} = 77$, $P < 0.001$), and the fit improvement by 3 CPT compared with 2 CPT was significant by F tests. However, the SEs of the V_T (lack of identifiability) associated with the fits were significantly higher for the 3-CPT model (%CV, 6.57% ± 15.42%) compared with the 2-CPT model (2.24% ± 1.52%; repeated-measures ANOVA: $F_{1,85} = 6.7$, $P = 0.01$). The SEs of the V_T were ≤10% in all 2-CPT fits. In contrast, 10 of 90 3-CPT fits were associated with SEs of the V_T that were >10%. Thus, adding the 4 nonconvergence cases to the 10 fits associated with low-parameter identifiability (%CV > 10%), the 3-CPT configuration failed to identify V_T values in 14 of 90 cases (16%).

Graphic analysis returned V_T values better correlated with the 2-CPT fit ($r^2 = 0.92$) than the 3-CPT fit ($r^2 = 0.84$). The regression of the graphic V_T to the 2-CPT V_T had a slope of 1.02 (95% confidence interval [CI], 0.96–1.08), whereas the regression of the graphic V_T to the 3-CPT V_T had a slope of 1.20 (95% CI, 1.09–1.31). Thus, the 3-CPT model, compared with the graphic and 2-CPT analyses, overestimated the V_T in regions with high V_T. V_T values were significantly different between the 3 methods (repeated-measures ANOVA: $F_{2,85} = 16$, $P < 0.001$). Posthoc analysis revealed that the 3-CPT V_T were significantly higher than the 2-CPT V_T ($P < 0.001$) and the graphic V_T ($P < 0.001$) but that the 2-CPT V_T and the graphic V_T were not significantly different ($P = 0.29$).

Figure 3A shows the V_T of all regions in the 6 subjects (n = 90) analyzed with 10 different scan durations ranging from 50 to 150 min (reference time) and the 2-CPT model. No significant bias (90% > V_T > 110%) was found for all durations >80 min. The error was tolerable (SD < 10%) for a scanning duration of >115 min. Similar results were obtained with the graphic analysis. In contrast, the 3-CPT method was unstable, with only a scan duration >125 min meeting these criteria. When considering the region with the highest V_T (MID), the time to reach stable V_T estimates according to these criteria was 140 min for 2-CPT analysis (Fig. 3B) and 130 min for graphic analysis, respectively. No duration shorter than the reference duration met these criteria for the MID V_T when the 3-CPT model was used.

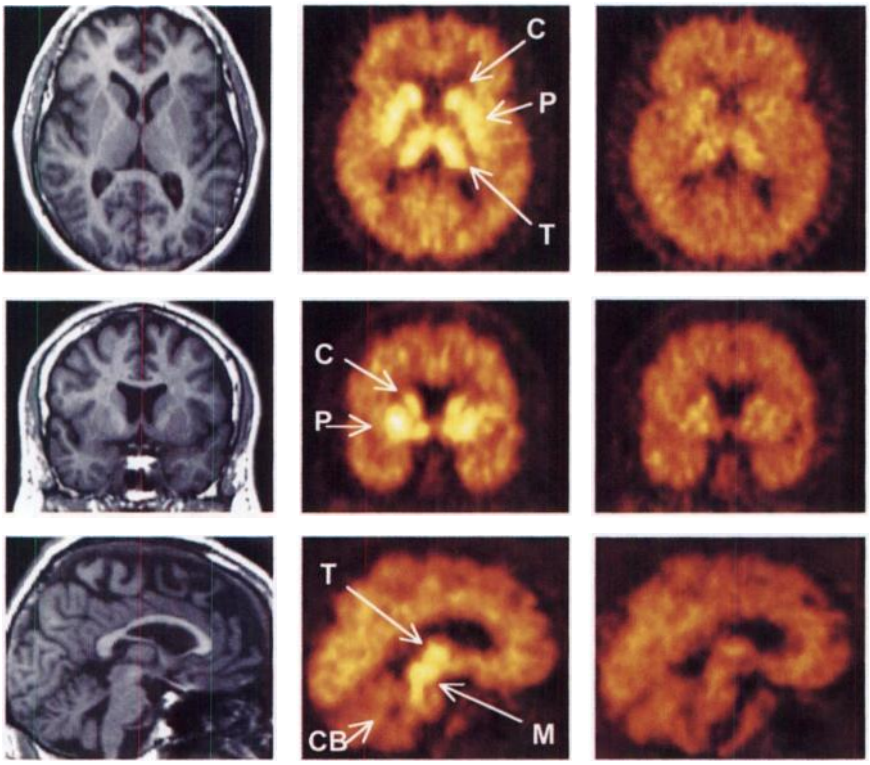

FIGURE 1. MR images (left column) and coregistered 10-min PET frames obtained from 70 to 80 min after injection of (+)-[^{11}C]McN 5652 (middle column) and (−)-[^{11}C]McN 5652 (right column). PET images are represented in a count-conservative manner, with same color scale and corrected for IDs. Transaxial (top row), coronal (middle row), and sagittal (bottom row) views are shown. At this time, increased activity concentrations in subcortical structures (C, caudate; P, putamen; T, thalamus; M, midbrain) are easily detectable. Activity in cortex is only marginally higher than that in cerebellum (CB) on (+) images.

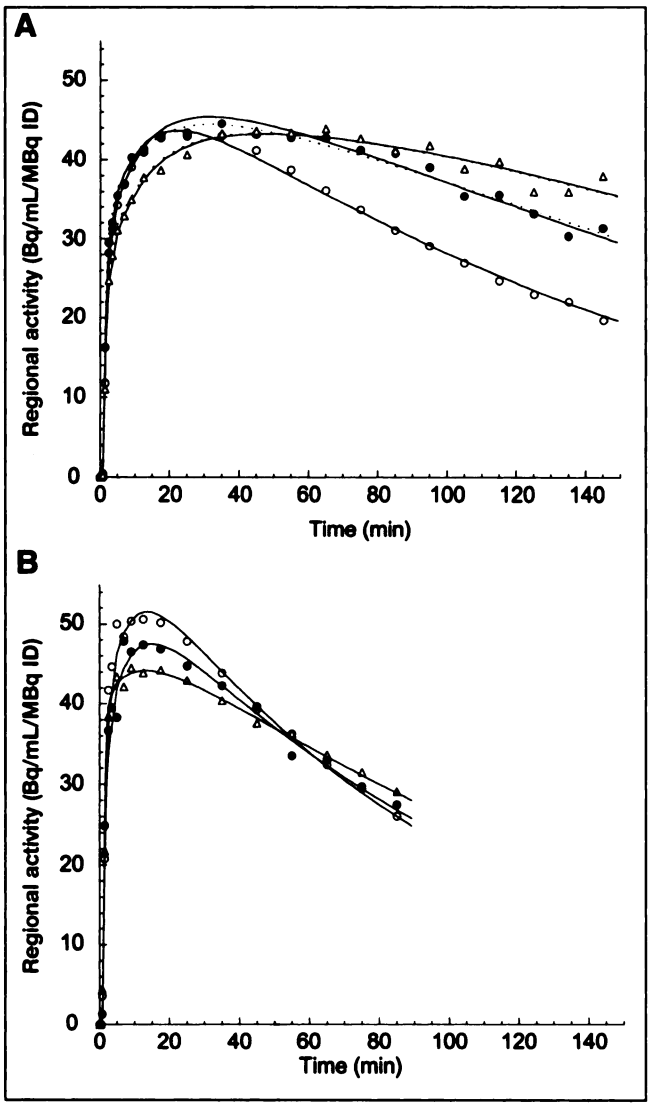

FIGURE 2. Time–activity curves in selected brain regions after injection of 688 MBq (+)-[^{11}C]McN 5652 (A) and 633 MBq (−)-[^{11}C]McN 5652 (B) in same human volunteer. Data were acquired for 150 min for (+)-[^{11}C]McN 5652 and 90 min for (−)-[^{11}C]McN 5652. x and y axes have been kept constant for both enantiomers to facilitate comparison. Brain regions depicted include CER (○), CAU (●), and MID (△). Symbols depict measured values, and continuous lines represent values fit to 2-CPT model. CAU and MID time–activity curves of (+)-[^{11}C]McN 5652 also include values fit to 3-CPT model as dotted lines, which are almost undistinguishable from 2-CPT fitted values (solid lines). CER, CAU, and MID (+)-[^{11}C]McN 5652 V_T were 16.6 mL/g, 24.3 mL/g, and 31.3 mL/g, respectively. CER, CAU, and MID (−)-[^{11}C]McN 5652 V_T were 10.7 mL/g, 10.9 mL/g, and 11.5 mL/g, respectively.

Significant between-region differences were observed in (+)-[^{11}C]McN 5652 V_T (2-CPT V_T ANOVA: $F_{14,75} = 13$, $P < 0.001$). Neocortical regions (DLPFC, MPFC, OFC, SPFC, ACC, TC, PC, and OC) had V_T values close to the cerebellar V_T. Six regions (AMY, HIP, CAU, PUT, THA, and MID) had V_T values significantly higher than the CER V_T (Fisher protected least significant difference [PLSD]; $P < 0.005$).

Brain Uptake of (−)-[^{11}C]McN 5652. In contrast to (+)-[^{11}C]McN 5652, the brain uptake of (−)-[^{11}C]McN 5652 was relatively uniform across regions (Figs. 1 and 2). (−)-[^{11}C]McN 5652 regional uptake was analyzed with 2-CPT and graphic analyses. Kinetic analysis with the 2-CPT model achieved convergence in all cases, and the V_T was identified with an error of 2.17% ± 1.01% (<10% in all cases). Results from both analyses were highly correlated ($r^2 = 0.98$; slope = 0.93; 95% CI, 0.91–0.96). Graphic analysis yielded values slightly but significantly higher than 2-CPT analysis (repeated-measures ANOVA: $F_{1,89} = 114$, $P < 0.001$). Analysis of the time dependency of the V_T by 2-CPT and graphic analyses revealed no major bias (90% < mean < 110%) at times later than 45 min and an acceptable error level (SD < 10%) for all scans longer than 25 min, indicating that 50 min of data are sufficient to derive the (−)-[^{11}C]McN 5652 V_T.

Despite the relatively uniform uptake, significant between-region differences were observed in (−)-[^{11}C]McN 5652 V_T (2-CPT V_T, ANOVA: $F_{14,75} = 3.3$, $P < 0.001$). Posthoc analysis revealed that 2 of 15 regions (THA and PUT) had a V_T significantly higher than the CER V_T (Fisher PLSD; $P < 0.05$).

Comparison of (+)- and (−)-[^{11}C]McN 5652 V_T. Comparison between (+)- and (−)-[^{11}C]McN 5652 V_T was performed with V_T values derived by 2-CPT modeling (Fig. 4). Table 2 lists the values of K_1, k_2, and V_T for both enantiomers and the ratio of (+) to (−) V_T. K_1 and k_2 values were significantly different between enantiomers. K_1 values of the active enantiomer were slightly higher than K_1 values of the inactive enantiomer (K_1 (+)-[^{11}C]McN 5652, 0.248 ± 0.37 mL/g/min; K_1 (−)-[^{11}C]McN 5652, 0.210 ± 0.56 mL/g/min; repeated-measures ANOVA: $F_{1,89} = 66$, $P < 0.001$), and k_2 values of the active enantiomer were half those of the inactive enantiomer (k_2 (+)-[^{11}C]McN 5652, 0.010 ± 0.003 min^{-1}; k_2 (−)-[^{11}C]McN 5652, 0.020 ±

TABLE 1
V_T of (+)-[^{11}C]McN 5652 in Human Brain

Region	2-CPT model	3-CPT model	Graphic
DLPFC	17.8 ± 3.0	19.6 ± 4.4	18.1 ± 3.1
MPFC	19.4 ± 3.5	20.7 ± 4.4	19.6 ± 3.8
OFC	18.4 ± 3.0	20.0 ± 4.5	18.5 ± 3.3
SPFC	23.6 ± 5.3	22.5 ± 6.6	23.2 ± 5.7
ACC	21.6 ± 3.5	23.2 ± 4.6	22.0 ± 4.2
TC	21.8 ± 3.9	22.1 ± 4.5	21.7 ± 4.1
PC	19.5 ± 3.2	20.9 ± 4.4	20.0 ± 3.9
OC	20.8 ± 3.2	22.3 ± 4.3	21.2 ± 3.6
AMY	37.7 ± 8.7	38.4 ± 8.9	33.6 ± 7.3
HIP	26.9 ± 9.1	32.0 ± 14.7	26.5 ± 9.9
CAU nucleus	33.3 ± 7.8	34.1 ± 8.0	32.0 ± 6.6
PUT	39.6 ± 8.1	47.1 ± 19.5	38.5 ± 8.5
THA	34.5 ± 7.2	36.1 ± 8.9	33.7 ± 7.7
MID	47.5 ± 12.7	52.4 ± 16.5	45.9 ± 12.8
CER	17.8 ± 1.9	21.9 ± 6.6	17.6 ± 2.1

Values are mean ± SD of V_T (mL/g) measured in 6 subjects.

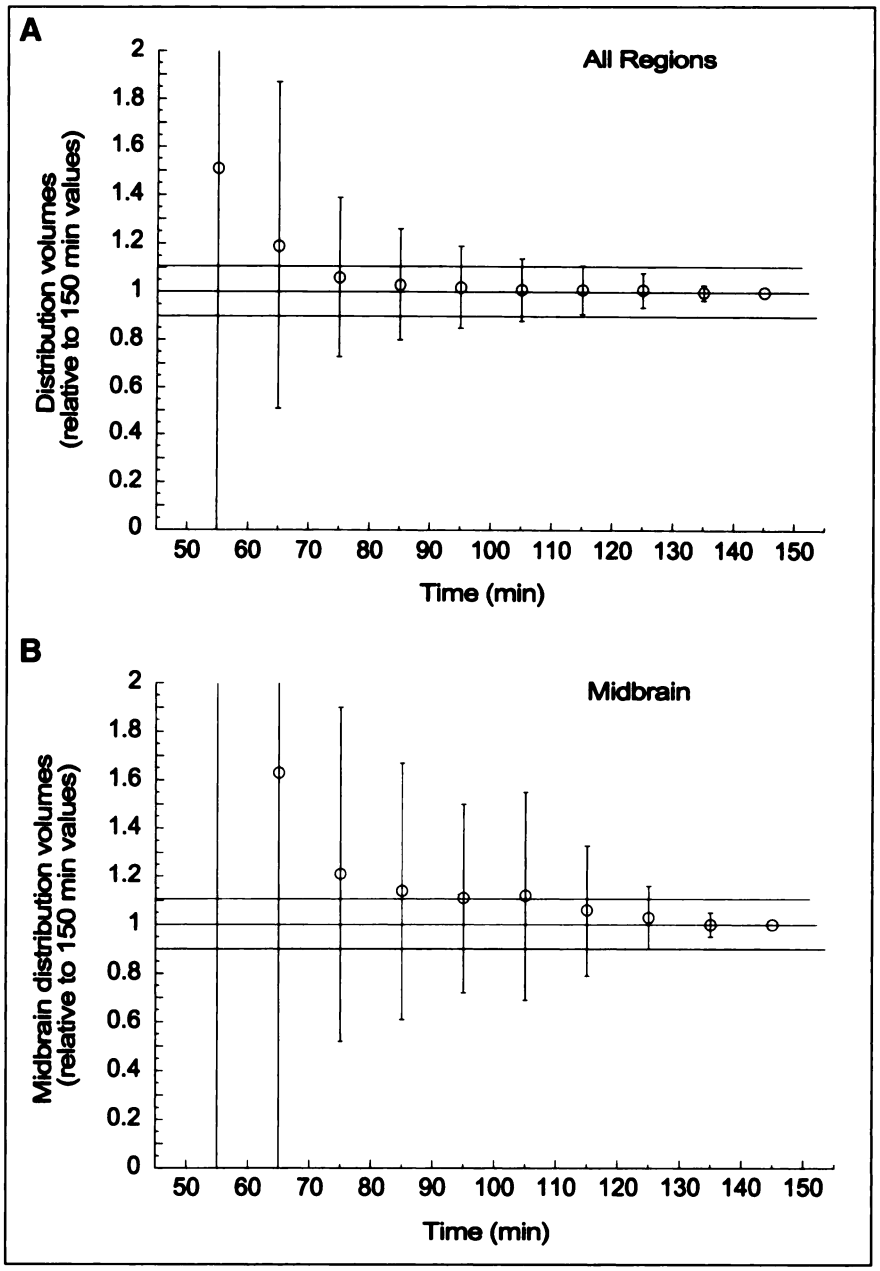

FIGURE 3. Time stability of (+)-[^{11}C]McN 5652 V_T derived with 2 CPT in all regions (A) and in MID (B). Times refer to midtimes of 10-min acquisitions. (A) V_T values (mean ± SD) as function of scanning duration of all regions in all subjects (n = 6 × 15 = 90), expressed relative to V_T values derived with 150-min scanning time (145 min as midtime of last 10-min acquisition). (B) MID V_T (mean ± SD) in all subjects (n = 6). Derivation from 100% of mean value indicates bias associated with shorter scanning time, whereas SD indicates error associated with shorter scanning time.

0.005 min^{-1}; repeated-measures ANOVA: $F_{1,89} = 279$, $P < 0.001$).

The differences between (+)- and (−)-[^{11}C]McN 5652 V_T were significant in every region, including the CER, a region devoid of 5-HT transporters. The significantly higher cerebellar (+) V_T compared with the (−) V_T (repeated-measures ANOVA: $F_{1,5} = 160$, $P < 0.001$) raised questions regarding the physiologic nature of the difference between the (+) and (−) V_T. More specifically, this observation suggested that the difference between the (+) and (−) V_T was not fully accounted for by the binding of (+)-[^{11}C]McN 5652 to 5-HT transporters. Blocking experiments were thus performed to clarify the nature of the difference between the (+) and (−) distribution volumes.

Blocking Experiments

Blocking Experiments in Baboon. Table 3 provides the V_T (2 CPT) measured in a baboon in 2 experiments. The first experiment was conducted under control conditions and included 1 injection of (+)-[^{11}C]McN 5652 followed by 1 injection of (−)-[^{11}C]McN 5652. The observation made in humans of higher (+) V_T in every region was replicated in this experiment. In cortical regions and the CER, the (+) V_T/(−) V_T ratio was 1.41 ± 0.04, a smaller difference than that observed in humans in the same regions (2.10 ± 0.20). This ratio was higher in the MID (2.37) and THA (2.04). In the second experiment, (−)-[^{11}C]McN 5652 was injected first. At the end of the (−)-[^{11}C]McN 5652 scan, citalopram was injected intravenously over 1 min (4 mg/kg, a dose

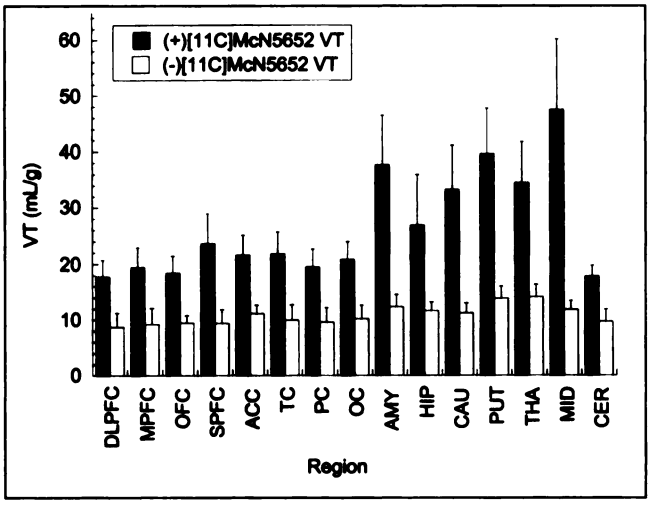

FIGURE 4. Comparison of (+)-[^{11}C]McN 5652 V_T ■ and (−)-[^{11}C]McN 5652 V_T □ under control conditions in healthy volunteers (n = 6). Values are mean ± SD. (+) V_T is significantly higher than (−) V_T in every region, including CER.

expected to fully saturate 5-HT transporters). (+)-[^{11}C]McN 5652 was injected 20 min after the citalopram injection. A clear reduction in (+)-[^{11}C]McN 5652 V_T was observed in the MID, THA, and striatum. In these regions, citalopram injection reduced the (+)-[^{11}C]McN 5652 V_T to V_T levels observed with (+)-[^{11}C]McN 5652 in the neocortical and cerebellar regions. In frontal, temporal, occipital, and cerebellar regions, citalopram failed to affect (+)-[^{11}C]McN 5652 V_T. In these regions, the (+) V_T/(−) V_T ratio was similar under citalopram pretreatment conditions (1.50 ± 0.04) compared with control conditions (1.41 ± 0.04). These results were replicated in a second experiment using 6 mg/kg intravenous citalopram (data not shown). These experiments indicated that no specific binding was detectable with (+)-[^{11}C]McN 5652 in neocortical and cerebellar regions of the baboon's brain. It was unclear if these results could be extrapolated to humans. In humans, the neocortical and cerebellar (+) V_T/(−) V_T ratio (2.10 ± 0.20) was higher than that in the baboons (1.41 ± 0.04), raising the possibility that (+)-[^{11}C]McN 5652 binding to 5-HT transporters might be detectable in these regions.

Blocking Experiments in Humans. A previously studied subject underwent a second experiment after pretreatment with 60 mg oral paroxetine. Table 4 presents the V_T under baseline and pretreatment conditions as well as the ratios of (+) V_T to (−) V_T. The test–retest reproducibility of this ratio under baseline conditions has not yet been assessed, but it is reasonable to postulate that changes of ≤10% are within the experimental variability. Decreases in (+) V_T/(−) V_T ratios exceeded 10% in the AMY, CAU, PUT, THA, and MID. Thus, in these regions, binding of (+)-[^{11}C]McN 5652 to 5-HT transporters was clearly detectable. In cortical and cerebellar regions, the differences between (+)- and (−)-[^{11}C]McN 5652 V_T were not affected by paroxetine, suggesting that, in these regions, this difference is not accounted for by binding of (+)-[^{11}C]McN 5652 to 5-HT transporters. These results were replicated in a second human subject using 80 mg paroxetine (data not shown).

Derivation of BP

Pretreatment experiments established that the difference between (+)- and (−)-[^{11}C]McN 5652 V_T does not provide an accurate measure of specific binding. On the other hand, (+)-[^{11}C]McN 5652 V_T in CER was essentially equal to the (+)-[^{11}C]McN 5652 nondisplaceable compartment (V_2). Therefore, BP was calculated as the difference between the regional (+)-[^{11}C]McN 5652 V_T and the CER (+)-

TABLE 2
(+)- and (−)-[^{11}C]McN 5652 in Human Brain: Comparison of Kinetic Parameters

	(+)-[^{11}C]McN 5652			(−)-[^{11}C]McN 5652			
Region	K_1 (mL/g/min)	k_2 (min^{-1})	V_T (mL/g)	K_1 (mL/g/min)	k_2 (min^{-1})	V_T (mL/g)	(+) V_T/(−) V_T ratio
DLPFC	0.24 ± 0.02	0.014 ± 0.002	17.8 ± 3.0	0.20 ± 0.06	0.023 ± 0.006	8.6 ± 1.9	2.2 ± 0.6
MPFC	0.26 ± 0.02	0.013 ± 0.002	19.4 ± 3.5	0.21 ± 0.07	0.022 ± 0.005	9.1 ± 2.2	2.3 ± 0.7
OFC	0.23 ± 0.02	0.013 ± 0.001	18.4 ± 3.0	0.18 ± 0.07	0.022 ± 0.004	8.5 ± 2.7	2.1 ± 0.4
SPFC	0.22 ± 0.02	0.010 ± 0.002	23.6 ± 5.3	0.17 ± 0.05	0.018 ± 0.004	9.4 ± 2.0	2.6 ± 0.7
ACC	0.26 ± 0.02	0.012 ± 0.001	21.6 ± 3.5	0.23 ± 0.03	0.022 ± 0.005	10.6 ± 1.6	2.0 ± 0.5
TC	0.22 ± 0.02	0.011 ± 0.001	21.8 ± 3.9	0.18 ± 0.05	0.018 ± 0.004	10.0 ± 2.1	2.3 ± 0.6
PC	0.26 ± 0.03	0.014 ± 0.002	19.5 ± 3.2	0.22 ± 0.07	0.023 ± 0.005	9.6 ± 2.0	2.1 ± 0.5
OC	0.28 ± 0.03	0.013 ± 0.002	20.8 ± 3.2	0.23 ± 0.06	0.023 ± 0.005	10.1 ± 1.8	2.1 ± 0.4
AMY	0.19 ± 0.02	0.005 ± 0.001	37.7 ± 8.7	0.17 ± 0.02	0.014 ± 0.003	12.4 ± 2.8	3.2 ± 1.1
HIP	0.22 ± 0.02	0.009 ± 0.002	26.9 ± 9.1	0.19 ± 0.02	0.017 ± 0.004	11.8 ± 2.7	2.4 ± 0.9
CAU nucleus	0.25 ± 0.02	0.008 ± 0.001	33.3 ± 7.8	0.22 ± 0.03	0.020 ± 0.005	11.4 ± 3.0	3.1 ± 1.0
PUT	0.31 ± 0.03	0.008 ± 0.001	39.6 ± 8.1	0.27 ± 0.03	0.020 ± 0.005	14.0 ± 3.1	3.0 ± 0.9
THA	0.29 ± 0.03	0.009 ± 0.001	34.5 ± 7.2	0.25 ± 0.02	0.019 ± 0.004	14.2 ± 3.4	2.5 ± 0.9
MID	0.23 ± 0.03	0.005 ± 0.001	47.5 ± 12.7	0.20 ± 0.02	0.017 ± 0.004	11.1 ± 1.6	4.1 ± 1.5
CER	0.25 ± 0.02	0.014 ± 0.002	17.8 ± 1.9	0.21 ± 0.05	0.022 ± 0.004	9.6 ± 1.7	1.9 ± 0.3

Values are mean ± SD measured in 6 subjects.

TABLE 3
Comparison Between (+)- and (−)-[^{11}C]McN 5652 V_T in Baboon Under Control and Blocked Conditions

Region	Control conditions			Citalopram* pretreatment†			Change in ratio (%)
	(+) V_T (mL/g)	(−) V_T (mL/g)	(+) V_T/(−) V_T ratio	(+) V_T (mL/g)	(−) V_T (mL/g)	(+) V_T/(−) V_T ratio	
MID	22.44	9.49	2.37	12.73	7.50	1.70	−39.4
THA	21.65	10.60	2.04	14.08	8.82	1.60	−27.5
TC	13.42	9.39	1.43	12.62	8.28	1.52	5.92
OC	11.69	8.14	1.44	10.51	7.22	1.46	1.37
CER	12.38	9.06	1.37	11.18	7.33	1.52	9.87

*4 mg/kg intravenously.
†For (+)-[^{11}C]McN 5652 only.
V_T values were derived with 2-CPT kinetic analysis.

[^{11}C]McN 5652 V_T (region-of-reference method). Table 5 lists BP values derived by the 2-CPT and graphic methods. BP values derived with both kinetic and graphic methods were highly correlated (r^2 = 0.94) and not statistically different from each other (repeated-measures ANOVA: $F_{1,89}$ = 1.8, P = 0.18).

Specific binding was defined as detectable in a given region if the regional BP values were significantly different from zero (1-sample t test). Specific binding was detected by both methods in the SPFC, ACC, TC, OC, AMY, HIP, CAU, PUT, THA, and MID. Both methods failed to detect specific binding in the DLPFC and OFC. Specific binding was detected by the graphic method, but not by 2-CPT model, in the MPFC and PC. Values of BP determined by the 2-CPT model are presented in Figure 5.

Like BP values, V_3'' values derived by both methods were highly correlated (r^2 = 0.96) and not statistically different (repeated-measures ANOVA: $F_{1,89}$ = 1.6, P = 0.20). V_3'' was not significantly different from zero in the DLPFC, MPFC, and OFC (Table 6).

DISCUSSION

In this study, the regional brain uptake of (+)- and (−)-[^{11}C]McN 5652 in humans was quantified using both kinetic and graphic analyses. As described previously (*8,29*), the regional patterns of uptake of (+)- and (−)-[^{11}C]McN 5652 were very different. Although (−)-[^{11}C]McN 5652 showed almost uniform distribution across brain regions, the uptake of (+)-[^{11}C]McN 5652 was more prominent in regions with high densities of 5-HT transporters, such as MID, THA, and basal ganglia. The goal of this investigation was to develop an appropriate method to derive 5-HT transporter BP from the analyses of the brain uptake of both enantiomers.

TABLE 4
Comparison Between (+)- and (−)-[^{11}C]McN 5652 V_T in Human Volunteer Under Control and Pretreatment Conditions

Region	Control conditions			Paroxetine* pretreatment			Change in ratio (%)
	(+) V_T (mL/g)	(−) V_T (mL/g)	(+) V_T/(−) V_T ratio	(+) V_T (mL/g)	(−) V_T (mL/g)	(+) V_T/(−) V_T ratio	
DLPFC	15.0	9.6	1.56	13.3	8.4	1.58	1.3
MPFC	16.6	10.2	1.63	14.6	9.2	1.58	−2.6
OFC	16.6	10.3	1.60	14.4	9.1	1.59	−0.9
SPFC	17.7	10.7	1.66	14.6	9.3	1.57	−5.5
ACC	18.9	11.2	1.68	16.2	10.1	1.60	−4.2
TC	17.7	10.9	1.62	15.3	9.7	1.58	−2.8
PC	16.9	10.9	1.56	15.5	9.5	1.63	4.6
OC	17.5	11.2	1.57	15.6	9.8	1.58	0.9
AMY	27.2	12.0	2.26	18.0	10.8	1.66	−26.8
HIP	18.9	11.1	1.70	15.8	9.5	1.66	−2.5
CAU nucleus	24.3	10.9	2.23	17.6	9.5	1.85	−16.9
PUT	29.9	14.4	2.08	22.3	12.7	1.76	−15.5
THA	26.5	13.8	1.92	20.1	12.2	1.64	−14.6
MID	31.3	11.5	2.71	16.8	10.0	1.69	−37.7
CER	16.6	10.7	1.55	14.7	9.3	1.58	1.8

*60 mg orally.
V_T values were derived with 2-CPT kinetic analysis.

TABLE 5
(+)-[^{11}C]McN 5652 BP: 2-CPT and Graphic Analyses

Region	2-CPT model BP (mL/g)	P	Graphic BP (mL/g)	P
DLPFC	−0.04 ± 1.38	NS	0.50 ± 1.36	NS
MPFC	1.64 ± 1.76	NS	1.97 ± 1.78	0.042
OFC	0.61 ± 1.37	NS	0.84 ± 1.48	NS
SPFC	5.85 ± 3.52	0.010	5.56 ± 3.70	NS
ACC	3.79 ± 1.74	0.003	4.43 ± 2.22	0.005
TC	3.99 ± 2.16	0.006	4.13 ± 2.15	0.005
PC	1.68 ± 1.45	NS	2.41 ± 1.93	0.028
OC	3.02 ± 1.49	0.004	3.61 ± 1.77	0.004
AMY	19.91 ± 7.00	<0.001	15.97 ± 5.43	<0.001
HIP	9.07 ± 7.92	0.038	8.84 ± 8.57	0.043
CAU nucleus	15.47 ± 6.11	0.002	14.37 ± 4.68	<0.001
PUT	21.85 ± 6.42	<0.001	20.94 ± 6.53	<0.001
THA	16.74 ± 5.45	<0.001	16.14 ± 5.74	0.001
MID	29.67 ± 11.01	0.001	28.32 ± 10.92	0.001

NS = not significant.
Values are mean ± SD (n = 6). BP was calculated as difference between (+) V_T in ROI and (+) V_T in CER; *P* gives probability for this difference to be significantly different from 0 (1-sample *t* test).

TABLE 6
(+)-[^{11}C]McN 5652 V_3'': 2-CPT and Graphic Analyses

Region	2 CPT model V_3'' (unitless)	P	Graphic V_3'' (unitless)	P
DLPFC	−0.01 ± 0.08	NS	0.02 ± 0.08	NS
MPFC	0.08 ± 0.10	NS	0.10 ± 0.10	0.047
OFC	0.03 ± 0.08	NS	0.04 ± 0.08	NS
SPFC	0.32 ± 0.17	0.006	0.30 ± 0.18	0.0094
ACC	0.21 ± 0.09	0.002	0.24 ± 0.10	0.0023
TC	0.22 ± 0.11	0.0042	0.23 ± 0.11	0.0033
PC	0.09 ± 0.08	0.038	0.13 ± 0.10	0.0255
OC	0.17 ± 0.07	0.0027	0.20 ± 0.09	0.0023
AMY	1.10 ± 0.31	<0.001	0.89 ± 0.22	<0.001
HIP	0.49 ± 0.42	0.0355	0.48 ± 0.45	0.0475
CAU nucleus	0.85 ± 0.28	<0.001	0.80 ± 0.19	<0.001
PUT	1.21 ± 0.27	<0.001	1.17 ± 0.25	<0.001
THA	0.92 ± 0.23	<0.001	0.90 ± 0.23	<0.001
MID	1.63 ± 0.48	<0.001	1.57 ± 0.46	<0.001

NS = not significant.
Values are mean ± SD (n = 6). V_3'' (equilibrium specific-to-nonspecific partition coefficient) was calculated as ratio of difference between (+) V_T in ROI and (+) V_T in CER to (+) V_T in CER; *P* gives probability for this difference to be significantly different from 0 (1-sample *t* test).

Comparison of the 2-CPT and 3-CPT models on several criteria revealed that the 2-CPT model provided a more reliable estimate of (+)-[^{11}C]McN 5652 V_T. Although the improvement in goodness of fit was statistically significant with 3 CPT compared with 2 CPT, this improvement was not apparent by visual inspection of the curves, suggesting that the kinetics of brain uptake were closely approximated by a 2-CPT model. Despite the increase in goodness of fit, several problems were associated with the 3-CPT model. First, in 4 of 90 fits, the 3 CPT failed to reach convergence criteria. Second, the identifiability of V_T by 3 CPT was significantly lower than by 2 CPT. An error on V_T > 10% was encountered in 10 of the 86 fits that reached convergence. Third, derivation of V_T by 3 CPT revealed a lack of time stability that was not observed in the 2-CPT analysis. Fourth, graphic analyses of [^{11}C]McN 5652 regional uptake produced V_T values closer to 2-CPT V_T than to 3-CPT V_T. Together, these data indicate that goodness of fit should not be the only criterion used to choose between models of increasing complexity and that the greater flexibility of 3 CPT compared with 2 CPT was associated with a unacceptable vulnerability to the experimental noise. We should also note that the 3-CPT model used to analyze these data was unconstrained. When we attempted to model the data using a 3-CPT model in which the K_1/k_2 ratio was constrained to the CER distribution volume, it failed to converge in 42 of 90 cases.

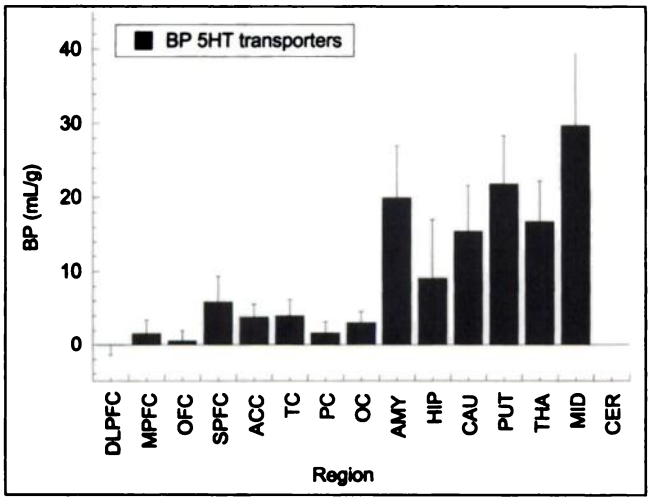

FIGURE 5. BP of (+)-[^{11}C]McN 5652 to 5-HT transporters in human brain (mean ± SD; n = 6). BP is calculated as difference between regional (+)-[^{11}C]McN 5652 V_T and CER (+)-[^{11}C]McN 5652 V_T.

The uptake of (+)-[^{11}C]McN 5652 in the MID, the region with highest density of 5-HT transporters, exhibited a kinetically distinct course; the peak activity occurred later and was more protracted than in the other brain regions. Relatively little washout was observed in the MID during the first 90 min of the experiment, raising concerns about the identifiability of the MID V_T after 90 min of data acquisition. Therefore, in these experiments, continuous scanning was obtained for 150 min. The combination of a relatively high ID, the high brain uptake of (+)-[^{11}C]McN 5652, and the greater sensitivity of the 3-dimensional scanning mode allowed the collection of meaningful data up to this late time. The availability of these extended datasets enabled us to define the minimal scan duration associated with an acceptable identifiability of MID V_T. Both the bias and the error had to be <10% to establish time stability. To meet

both criteria in every region, a minimum of 140 min was needed. The need of such a long scanning time represents a limitation of this radiotracer, both in terms of counting statistics and of patient compliance.

Consistent with a measure of nonspecific binding, the brain uptake of (−)-[^{11}C]McN 5652 was relatively uniform across regions, although uptake in the THA and PUT was slightly, but significantly, higher than cortical uptake. This observation raised the possibility of a weak binding of (−)-[^{11}C]McN 5652 to 5-HT transporters. However, the MID (−)-[^{11}C]McN 5652 V_T was comparable with the CER (−)-[^{11}C]McN 5652 V_T. Therefore, the higher (−)-[^{11}C]McN 5652 V_T observed in THA and PUT is more likely associated with regional differences in nonspecific binding.

We expected that both enantiomers would display similar levels of nonspecific binding and that the V_T of both enantiomers would be similar to that in the CER, a region devoid of 5-HT transporters (V. Arango, M. Underwood, oral communication, June 1999) (*30–32*). However, in every subject, the cerebellar V_T of (+)-[^{11}C]McN 5652 was almost double the V_T of cerebellar (−)-[^{11}C]McN 5652 (mean ratio, 1.9 ± 0.3). The consistent observation of a lower (−) V_T compared with the (+) V_T in the CER was thus an unexpected finding of this study.

Blocking experiments were required to further investigate the nature of the difference between the (+) and (−) cerebellar V_T. Although citalopram and paroxetine decreased the (+) V_T in several subcortical regions such as the MID, no effect of these drugs was apparent on the (+) V_T in neocortical regions and in the CER. If the difference between the (+) and (−) V_T corresponded to binding of (+)-[^{11}C]McN 5652 to 5-HT transporters in the CER and neocortex, pretreatment with citalopram or paroxetine should significantly reduce the (+) V_T/(−) V_T ratio in these regions. Because no reduction of cerebellar or neocortical (+) V_T/(−) V_T was observed, these blocking experiments showed that the difference between the (+) and (−) V_T in cortex and CER was not associated with binding of (+)-[^{11}C]McN 5652 to 5-HT transporters.

The nature of the nondisplaceable component of the difference between (+)- and (−)-[^{11}C]McN 5652 V_T is unknown. (+)-[^{11}C]McN 5652 might specifically bind to a yet unidentified brain protein that would be relatively uniformly distributed across brain regions. (+)-[^{11}C]McN 5652 displays a non-negligible affinity for the norepinephrine and dopamine transporters (*6*). Yet, these transporters are unlikely candidates to explain the component of the difference between the (+) and (−) V_T that is unaffected by selective 5-HT blockers: Saturating doses of the norepinephrine uptake inhibitor desimipramine and of the dopamine uptake inhibitor GBR 12935 did not affect (+)-[^{11}C]McN 5652 brain uptake in the rat (*4*), and the relative uniform distribution of this putative site does not match the highly selective distribution of norepinephrine and dopamine transporters (*33,34*). On the other hand, the nondisplaceable difference between (+)- and (−)-[^{11}C]McN 5652 V_T might stem from a difference in the plasma-free fraction (f_1). If the (+)-[^{11}C]McN 5652 f_1 was higher than the (−)-[^{11}C]McN 5652 f_1, the tissue distribution volume of (+)-[^{11}C]McN 5652 relative to total plasma parent would be higher than that of (−)-[^{11}C]McN 5652. Because the high binding of [^{11}C]McN 5652 to the ultracentrifugation filters prevented accurate measurement of f_1, this hypothesis could not be tested.

Although the nature of the nondisplaceable difference between (+)- and (−)-[^{11}C]McN 5652 V_T remains to be elucidated, its implication for the measurement of 5-HT transporter BP is clear: The difference between the distribution volume of both enantiomers should not be used to estimate 5-HT transporter BP. The use of the difference between the (+) and (−) V_T to define nonspecific binding yields an overestimation of specific binding. This overestimation would be particularly important in neocortical regions. Because this method was used in the measurement of 5-HT transporters in chronic *N*-methyl-D-asparate abusers, the results of this study should be viewed with caution (*35*).

The (+)-[^{11}C]McN 5652 V_T in the CER is a more appropriate index of the nondisplaceable distribution volume of (+)-[^{11}C]McN 5652. First, this region is devoid of 5-HT transporters. Second, saturation experiments in baboon reduced the distribution volumes in receptor-rich regions to the level observed in the CER. Therefore, BP was calculated as the difference between the regional (+)-[^{11}C]McN 5652 V_T and the cerebellar (+)-[^{11}C]McN 5652 V_T.

Because cerebellar (+)-[^{11}C]McN 5652 V_T was comparable with neocortical (+)-[^{11}C]McN 5652 V_T, it follows that BP in neocortical regions was extremely low. In fact, in several regions such as DLPFC, MPFC, and OFC, BP values were not significantly different from zero. In other neocortical regions, this value was small but significantly different from zero. However, because BP in these regions is a small number calculated by the difference between 2 large numbers, this measurement is less reliable. The only neocortical region associated with BP > 5 was the SPFC, which is interesting in view of the implication of this region in familial depression (*36,37*).

The small to negligible BP measured with (+)-[^{11}C]McN 5652 in neocortical regions appears at odds with the well-documented presence of 5-HT transporters in these regions (*38*). Using [^{3}H]paroxetine, the density of 5-HT transporters was estimated to be 60–80 fmol/mg P in the prefrontal cortex (*30*). We believe that the very high nonspecifc binding of (+)-[^{11}C]McN 5652 might result in a signal-to-noise ratio too low for reliable detection of the specific signal in the prefrontal cortex. The nonspecific distribution volume of (+)-[^{11}C]McN 5652 was 17.8 ± 1.9 mL/g. By comparison, the nonspecific distribution volume of the D_1 receptor radiotracer [^{11}C]NNC 112 measured in the same setting is 2.5 ± 0.4 mL/g in humans (n = 6)—that is, about 10 times lower than that of (+)-[^{11}C]McN 5652 (*14*). The nonspecific distribution volume of the 5-HT_{1A} antagonist [^{11}C]WAY 100635 is 0.6 ± 0.2 mL/g (n = 4)—that is,

about 30 times lower (R. Parsey, unpublished data, January 1999). These comparisons highlight the very high nonspecific binding of [^{11}C]McN 5652.

Despite this high nonspecific binding, specific binding could be readily quantified in regions with high BP (BP range, 10–50 mL/g), such as in the medial temporal structures (AMY and HIP), basal ganglia, THA, and MID. These observations are consistent with the high densities of 5-HT transporters observed in these regions (range, 150–600 fmol/mg protein) (*30*).

CONCLUSION

Both 2-CPT kinetic and graphic analyses of (+)-[^{11}C]McN 5652 uptake provided appropriate quantitative methods for the measurement of 5-HT transporter BP in limbic, striatal, thalamic, and MID regions of the living human brain. Measurement of (−)-[^{11}C]McN 5652 distribution volume is neither needed nor desirable for derivation of (+)-[^{11}C]McN 5652 BP. The major limitations of this radioligand are the high nonspecific binding, precluding reliable measurement of 5-HT transporters in the human neocortex, and the prolonged scanning time needed to derive a stable outcome measure. Despite its limitations, (+)-[^{11}C]McN 5652 enables in vivo quantification of 5-HT transporters in several important regions. The reproducibility of this quantification is of critical importance and remains to be determined. The only alternative radioligand currently available in humans is [^{123}I]β-CIT, which allows only for measurement of 5-HT transporters in the MID area (*27*). For example, using [^{123}I]β-CIT, Malison et al. (*39*) reported a reduced availability of 5-HT transporters in the MID of patients with major depression, and Heinz et al. (*40*) reported reduced MID 5-HT transporter availability in patients with alcoholism. PET studies with (+)-[^{11}C]McN 5652 will permit replication of these observations and extension of these investigations to other brain regions. Although (+)-[^{11}C]McN 5652 will be valuable to study 5-HT transporters in depression and other neuropsychiatric conditions, additional research is warranted to develop a radioligand with lower nonspecific binding and a faster kinetic profile.

ACKNOWLEDGMENTS

The authors thank Zsolt Szabo, MD, and Chester A. Mathis, PhD, for providing toxicology and dosimetry information for [^{11}C]McN 5652; and Ning-Ning Guo, PhD, Ilise Lombardo, MD, Yolanda Zea-Ponce, PhD, Yiyun Huang, PhD, as well as the technical staff of the brain imaging division (Analia Arevalo, Suehee Chung, Julie Montoya, Justine Pidcock, Dan Schneider, Ann Shinn, Bryan Bergert, and Richard Weiss) and of the Kreitchman PET Center at Columbia University for expert assistance. This work was supported by U.S. Public Health Service grants NIMH P30-MH46745, NIMH P30-MH40695, and NIMH K02-MH01603.

REFERENCES

1. Lucki I. The spectrum of behaviors influenced by serotonin. *Biol Psychiatry.* 1998;44:151–162.
2. Deakin JF. The role of serotonin in panic, anxiety and depression. *Int Clin Psychopharmacol.* 1998;13(suppl 4):S1–S5.
3. Habert E, Graham D, Tahraoui L, Claustre Y, Langer SZ. Characterization of [^{3}H]paroxetine binding to rat cortical membranes. *Eur J Pharmacol.* 1985;118:107–114.
4. Suehiro M, Scheffel U, Dannals RF, Ravert HT, Ricaurte GA, Wagner H Jr. A PET radiotracer for studying serotonin uptake sites: carbon-11-McN-5652Z. *J Nucl Med.* 1993;34:120–127.
5. Suehiro M, Scheffel U, Ravert HT, Dannals RF, Wagner H Jr. [^{11}C](+)McN5652 as a radiotracer for imaging serotonin uptake sites with PET. *Life Sci.* 1993;53:883–892.
6. Shank RP, Vaught JL, Pelley KA, Setler PE, McComsey DF, Maryanoff BE. McN-5652: a highly potent inhibitor of serotonin uptake. *J Pharmacol Exp Ther.* 1988;247:1032–1038.
7. Szabo Z, Scheffel U, Suehiro M, et al. Positron emission tomography of 5-HT transporter sites in the baboon brain with [^{11}C]McN5652. *J Cereb Blood Flow Metab.* 1995;15:798–805.
8. Szabo Z, Kao PF, Scheffel U, et al. Positron emission tomography imaging of serotonin transporters in the human brain using [^{11}C](+)McN5652. *Synapse.* 1995;20:37–43.
9. Abi-Dargham A, Simpson N, Kegeles L, et al. PET studies of binding competition between endogenous dopamine and the D1 radiotracer [^{11}C]NNC 756. *Synapse.* 1999;32:93–109.
10. Suehiro M, Musachio JL, Dannals RF, et al. An improved method for the synthesis of radiolabeled McN5652 via thioester precursors. *Nucl Med Biol.* 1995;22:543–545.
11. Wienhard K, Eriksson L, Grootoonk S, Casey M, Pietrzyk U, Heiss WD. Performance evaluation of the positron scanner ECAT EXACT. *J Comp Assist Tomgr.* 1992;16:804–813.
12. Abi-Dargham A, Laruelle M, Seibyl J, et al. SPECT measurement of benzodiazepine receptors in human brain with [^{123}I]iomazenil: kinetic and equilibrium paradigms. *J Nucl Med.* 1994;35:228–238.
13. Gandelman MS, Baldwin RM, Zoghbi SS, Zea-Ponce Y, Innis RB. Evaluation of ultrafiltration for the free fraction determination of single photon emission computerized tomography (SPECT) radiotracers: β-CIT, IBF and iomazenil. *J Pharm Sci.* 1994;83:1014–1019.
14. Abi-Dargham A, Martinez D, Mawlawi O, et al. Measurement of striatal and extrastriatal dopamine D1 receptor binding potential with [^{11}C]NNC 112 in humans: validation and reproducibility. *J Cereb Blood Flow Metab.* In press.
15. Woods RP, Cherry SR, Mazziotta JC. Rapid automated algorithm for aligning and reslicing PET images. *J Comp Assist Tomogr.* 1992;16:620–633.
16. Duvernoy H. *The Human Brain: Surface, Three-Dimensional Sectional Anatomy and MRI.* New York, NY: Springer-Verlag; 1991.
17. Talairach J, Tournoux P. *Co-Planar Stereotactic Atlas of the Human Brain: Three-Dimensional Proportional System—An Approach of Cerebral Imaging.* New York, NY: Theime Medical; 1988.
18. Killiany RJ, Moss MB, Nicholson T, Jolez F, Sandor T. An interactive procedure for extracting features of the brain from magnetic resonance images: the lobes. *Hum Brain Mapp.* 1997;5:355–363.
19. Kates WR, Abrams MT, Kaufmann WE, Breiter SN, Reiss AL. Reliability and validity of MRI measurement of the amygdala and hippocampus in children with fragile X syndrome. *Psychiatr Res Neuroimag.* 1997;75:31–48.
20. Mintun MA, Raichle ME, Kilbourn MR, Wooten GF, Welch MJ. A quantitative model for the in vivo assessment of drug binding sites with positron emission tomography. *Ann Neurol.* 1984;15:217–227.
21. Laruelle M, Baldwin RM, Rattner Z, et al. SPECT quantification of [^{123}I]iomazenil binding to benzodiazepine receptors in nonhuman primates. I. Kinetic modeling of single bolus experiments. *J Cereb Blood Flow Metab.* 1994;14:439–452.
22. Koeppe RA, Holthoff VA, Frey KA, Kilbourn MR, Kuhl DE. Compartmental analysis of [^{11}C]flumazenil kinetics for the estimation of ligand transport rate and receptor distribution using positron emission tomography. *J Cereb Blood Flow Metab.* 1991;11:735–744.
23. Akaike H. A new look at the statistical model identification. *IEEE Trans Automat Contr.* 1974;AC19:716–723.
24. Landlaw EM, DiStefano JJ III. Multiexponential, multicompartmental, and noncompartmental modeling. II. Data analysis and statistical considerations. *Am J Physiol.* 1984;246:R665–R677.
25. Carson RE. Parameters estimation in positron emission tomography. In: Phelps ME, Mazziotta JC, Schelbert HR, eds. *Positron Emission Tomography: Principles*

and Applications for the Brain and the Heart. New York, NY: Raven Press; 1986:347–390.
26. Logan J, Fowler J, Volkow ND, et al. Graphical analysis of reversible radioligand binding from time-activity measurements applied to [*N*-^{11}C-methyl]-(−)-cocaine PET studies in human subjects. *J Cereb Blood Flow Metab*. 1990;10:740–747.
27. Laruelle M, Baldwin RM, Malison RT, et al. SPECT imaging of dopamine and serotonin transporters with [^{123}I]β-CIT: pharmacological characterization of brain uptake in nonhuman primates. *Synapse*. 1993;13:295–309.
28. McClelland GR, Raptopoulos P. EEG and blood level of the potential antidepressant paroxetine after a single oral dose to normal volunteers. *Psychopharmacology*. 1984;83:327–329.
29. Szabo Z, Kao PF, Mathews WB, et al. Positron emission tomography of 5-HT reuptake sites in the human brain with C-11 McN5652 extraction of characteristic images by artificial neural network analysis. *Behav Brain Res*. 1996;73:221–224.
30. Laruelle M, Vanisberg M, Maloteaux J. Regional and subcellular localization in human brain of [^{3}H]paroxetine binding, a marker of serotonin uptake sites. *Biol Psychiatry*. 1988;24:299–309.
31. Cortes R, Soranoi E, Pazos A, Probst A, Palacios JM. Autoradiography of antidepressant binding sites in the human brain: localization using [^{3}H]imipramine and [^{3}H]paroxetine. *Neuroscience*. 1988;27:473–496.
32. Bäckström I, Bergström M, Marcusson J. High affinity [^{3}H]paroxetine binding to serotonin uptake sites in human brain tissue. *Brain Res*. 1989;486:261–268.
33. Charnay Y, Leger L, Vallet PG, Hof PR, Jouvet M, Bouras C. [^{3}H]nisoxetine binding sites in the cat brain: an autoradiographic study. *Neuroscience*. 1995;69:259–270.
34. Marcusson J, Erikson K. [^{3}H]GBR-12935 binding to dopamine uptake sites in the human brain. *Brain Res*. 1988;457:122–129.
35. McCann UD, Szabo Z, Scheffel U, Dannals RF, Ricaurte GA. Positron emission tomographic evidence of toxic effect of MDMA ("Ecstasy") on brain serotonin neurons in human beings. *Lancet*. 1998;352:1433–1437.
36. Drevets WC, Price JL, Simpson JR Jr, et al. Subgenual prefrontal cortex abnormalities in mood disorders. *Nature*. 1997;386:824–827.
37. Mayberg HS, Liotti M, Brannan SK, et al. Reciprocal limbic-cortical function and negative mood: converging PET findings in depression and normal sadness. *Am J Psychiatry*. 1999;156:675–682.
38. Arango V, Underwood MD, Gubbi AV, Mann JJ. Localized alterations in pre- and postsynaptic serotonin binding sites in the ventrolateral prefrontal cortex of suicide victims. *Brain Res*. 1995;688:121–133.
39. Malison RT, Price LH, Berman R, et al Reduced brain serotonin transporter availability in major depression as measured by [^{123}I]-2 beta-carbomethoxy-3 beta-(4-iodophenyl)tropane and single photon emission computed tomography. *Biol Psychiatry*. 1998;44:1090–1098.
40. Heinz A, Ragan P, Jones DW, et al. Reduced central serotonin transporters in alcoholism. *Am J Psychiatry*. 1998;155:1544–1549.